

國立臺灣大學工學院材料科學與工程學系

博士論文

Department of Materials Science and Engineering

College of Engineering

National Taiwan University

Doctoral Dissertation

高強度Al-Cu-Mg-(Ag)鋁合金與輕量化CoCrNi-(Si)中熵合金  
之顯微結構與機械性質研究

**Microstructures and Mechanical Properties Investigations on  
High-Strength Al-Cu-Mg-(Ag) Aluminum Alloys and Light-  
Weight CoCrNi-(Si) Medium Entropy Alloys**

戴正凌

Cheng-Ling Tai

指導教授：楊哲人 博士

Advisor: Jer-Ren Yang, Ph.D.

中華民國 113 年 7 月

July 2024

國立臺灣大學博士學位論文  
口試委員會審定書

DOCTORAL DISSERTATION ACCEPTANCE CERTIFICATE  
NATIONAL TAIWAN UNIVERSITY

(論文中文題目) 高強度 Al-Cu-Mg-(Ag) 鋁合金與輕量化  
(Chinese title of Doctor's Thesis) CoCrNi-(Si) 中熵合金之顯微結構與機械性質研究

(論文英文題目) Microstructures and Mechanical Properties  
(English title of Doctor's Thesis) Investigations on High-Strength Al-Cu-Mg-(Ag)  
Aluminum Alloys and Light-Weight CoCrNi-(Si)  
Medium Entropy Alloys

本論文係 **戴正凌** F08527007 在國立臺灣大學材料科學與工程學系完成之博士學位論文，於民國 113 年 07 月 29 日承下列考試委員審查通過及口試及格，特此證明。

The undersigned, appointed by the Department / Graduate Institute of Materials Science and Engineering on 29 July 2024 have examined a Doctoral Dissertation entitled above presented by **Cheng-Ling Tai** F08527007 candidate and hereby certify that it is worthy of acceptance.

口試委員  
Oral examination committee:

楊哲人 楊哲人  
(指導教授 Advisor)

李勝隆 李勝隆

蕭健男 蕭健男

王涵聖 王涵聖

陳志遠 陳志遠

蘇德徵 蘇德徵

鍾采甫 鍾采甫

(所、學位學程) 主管 Director: 蔡豐羽 蔡豐羽

## 誌謝

不知不覺進入 PT group 已經過了五年。首先不免俗但依舊真誠地感謝我父母戴先生和邱小姐在我說出我想讀博班時沒有一絲一毫地反對或質疑，相反地，支持我讓我放手做想做的事，也因此成就了已經 27 歲但還是充滿學生氣息的我。再來特別感謝楊哲人老師在我一開始接觸實驗室時就熱情地跟我介紹雙晶，並帶領我進入原子級的世界，並且在我申請各種國外實習與研討會時無條件支持我，以及常常被我追著修改 paper，成就了看似履歷很好的我，十分榮幸能加入老師的實驗室。再來就是鋁合金戰隊老大采甫學長，陰錯陽差之下被學長說服做鋁合金，從一開始 TEM 的教學到後續申請獎學金以及發表 paper 技巧，從學長身上學到了許多，之後在請鍾教授多指教。接著是一進來實驗室帶著我們做實驗的佑誼、思妤及昱維，感謝你們協助我們學習實驗室的各種儀器及考古題支援，讓我們開心度過碩一菜鳥期。再來是梓敬學長，雖然在讀博班之後變學弟了，但你是我遇到實驗、課業及各種問題時第一個想到能諮詢的人，有曹博在的實驗室特別令人放心，如今雖然我走了但你還在哈哈，請你趕快畢業。柏翰學長身為實驗室大柱子跟材料系八卦中心帶著我們嘗試各種實驗，到後來變成 spectra 300 博後，總是能讓我放心不調光直接使用，可惜事務繁忙偶爾會覺得少了你的幽默。接著就是同期的一堆人了，首先是逕博同胞家俊跟仕淵，你們兩個先逕博是我逕博的原因之一，事實也證明有兩個給力又能一起歡笑的伙伴多麼重要，認識你們是我讀博班最大的收穫之一，雖然

疫情讓我們前期都沒辦法出國開會，但每次說走就走的吃貨行程還是歷歷在目，幸好後期除了出國開會，偶爾也會相約出國。銘奕、有銘、侑霖及宥瑄碩一同期們請好好檢討，都要找以前的誌謝才想起你們的名字怎麼寫，懷念跟你們一起修課跟做實驗的日子，或者其實沒有，銘奕先在這邊感謝你幫我寫歌了。學弟妹們家豪、承哲、忠威、伯叡、廷融、宜嫻、炯源、冠名、翔琳、書誠、泓任、雨蓁和詩雅，有因為疫情也有因為後來我大部分都在國外，跟各位相處時間比較少，但還是很開心認識你們，祝大家畢業後都順利賺大錢。這邊多感謝一下書誠好了，謝謝你都會把我實驗上的想法加以實踐，即使有時候工作量很大，都還是開心(?)去做出完整的分析。感謝系辦各位在需要時幫我處理許多事情及陳先生呂小姐賢伉儷在實驗上與報帳上幫助我許多。最後感謝女友書嫻陪伴我度過艱難(?)的博士生涯，陪我寫paper 陪我吃喝玩樂甚至陪我到國外實習，寫少一點免得審核不通過，希望你之後不要跟我分手讓我這段成為把柄。

另外感謝各個口委李勝隆教授、鍾采甫教授、蕭健男博士、蘇德徵教授、陳志遠教授及王涵聖博士提出了許多建議讓我能做修正並有所進步。還有感謝多次讓我去 NIMS 實習的 Ohmura 教授及幫我做無數臨場變形 TEM 實驗地 li-san，雖然你們看不懂，但還是謝謝你們的幫助讓我完成這本博士論文。並感謝財團法人國防工業發展基金會提供獎學金讓我能專注於實驗。

## 中文摘要

本研究探討材料之微觀結構與機械性質之間關連性，主要以鋁合金與中熵合金作為研究對象。鋁合金採用二系列鋁合金(Al-Cu-Mg)，研究添加微量 Ag 與否對各個時效階段中析出物之形成與材料強度之影響。透過穿透式電子顯微鏡(Transmission Electron Microscope, TEM)觀察時效初期、尖峰時效、過時效與長時間時效之析出物演化過程，如尺寸、形貌與分布情形。並藉由高解析掃描穿透式電子顯微鏡(High Resolution- Scanning Transmission Electron Microscope, HR-STEM)解析奈米析出物之原子級結構，深入了解各個析出物，搭配電子能量損失光譜(EELS)定量分析析出物之體積佔比。接著透過拉伸試驗測試個時效階段之機械性質，結合微結構分析，深入了解析出物對材料機械性質之影響。

研究發現，添加 Ag 後產生之  $\Omega$  相能大幅提升材料強度。除了本身具有熱穩定性外， $\Omega$  相的形成能在 11 小時至 18 小時階段抑制 S 相粗化，使材料於過時效階段能維持強度。透過研究團簇物發現，其原因為大量生成之  $\Omega$  相能加速消耗鋁基地中的 Cu-Mg 團簇物，使 S 相不易粗化。透過此實驗發現  $\Omega$  相與 S 相之競爭關係，故進一步研究了 AA2040 Al-5.1Cu-1.0Mg-0.4Ag 高強度鋁合金中，其於不同時效時間點進行溫成形模擬對材料顯微結構與機械性質所造成之影響，觀察何種熱處理將表現出最佳性質。時效溫度 200 °C 下分別於時效前 (5 %-1h)、預時效 20 分鐘 (20 min-5 %-40 min)、40 分鐘 (40 min-5 %-20 min)與時效結束後進行 5 %壓縮

變形 (1h-5%)，四種條件總時效時間均為一小時，觀察其強度變化與對應微結構。結果顯示與一般時效強化材料相反，時效前之變形會降低此材料強度。透過  $\Omega$  相體積分率與 S 相數量分率統計發現，時效前進行變形將抑制  $\Omega$  相生成，導致強度下降。而 40 min-5%-20 min 表現出最高強度，表示於時效後期進行溫成形模擬，能導入差排加速後續時效中 S 相析出，且時效時間短不會導致粗化，結合  $\Omega$  相貢獻，將達到最高強度。

本論文下半部分為 CoCrNi 中熵合金之研究。由於其低溫下能以變形雙晶作為變形手段，故有極佳強度與延展性，可應用於極地抑或是太空中。本研究探討了添加矽將此材料輕量化之餘，其對圍觀結構與機械性質之影響，主要利用臨場變形穿透式電子顯微鏡(in-situ TEM)進行研究。研究發現添加矽能有效降低疊差能。相較於 CoCrNi 中熵合金於 110 方向單晶變形以差排滑移作為主要機制，CoCrNi-Si 中熵合金能於降伏強度後產生變形雙晶阻礙差排移動，提升加工硬化率。此外，由於目前極具爭議之短距有序結構是否對強度提升有幫助，本實驗透過 in-situ TEM 對此進行研究。發現均勻分布之短距有序結構能使 CoCrNi 中熵合金整體變形均勻，並且於劇烈變形後產生變形雙晶，有效提升材料強度

關鍵字：AA2024 鋁合金、微量銀添加、熱穩定  $\Omega$  相、S 相、溫成形、高解析掃描式穿透電子顯微鏡、CoCrNi 中熵合金、矽添加、臨場壓縮穿透式電子顯微鏡、短距有序結構、變形雙晶

## Abstract

In this dissertation, the study explores the correlation between microstructure and mechanical properties of materials, with a primary focus on aluminum alloys and medium entropy alloys. The research specifically delves into the examination of 2xxx aluminum alloys (Al-Cu-Mg) and assesses the impact of introducing minor quantities of Ag on precipitate formation and material strength throughout various stages of the ageing process. The observations of precipitate evolution, size, morphology, and distribution, were conducted using Transmission Electron Microscopy (TEM) at early, peak, over-ageing, and prolonged ageing stages. The atomic structure of nano-precipitates was analyzed through High-Resolution Scanning Transmission Electron Microscopy (HR-STEM), and the volume fraction of precipitates was quantitatively assessed using EELS. Mechanical properties were evaluated at each stage through tensile tests, establishing correlations with microstructural analyses to comprehend the strengthening effects of distinct precipitates on the alloys.

The present study reveals that the introduction of Ag results in the significant enhancement of material strength, primarily attributed to the formation of the  $\Omega$  phase. The  $\Omega$  phase, besides demonstrating thermal stability, effectively consumes abundant Cu-Mg clusters, thereby impeding the coarsening of the S phase from 11 hours to 18 hours, consequently maintaining material strength during the over-ageing stage. The competitive relationship between the  $\Omega$  phase and S phase is identified, leading to an exploration of the effects of simulated warm forming at different ageing timings on the microstructure and mechanical properties of the AA2040 Al-5.1Cu-1.0Mg-0.4Ag high-strength aluminum alloy. Four distinct combinations of warm forming and artificial ageing (5%+1h, 20 min+5%+40 min, 40 min+5%+20 min, and 1h+5%) were examined to

observe the strength improvement and corresponding microstructure. In contrast to conventional age-hardening materials, pre-strain resulted in reduced the alloy's strength. The study concludes that the 40 min+5%+20 min sample exhibited the highest strength, attributed to the combined effects of  $\Omega$  and S phases.

The subsequent section of this dissertation focuses on the equiatomic CoCrNi medium entropy alloy (MEA). This alloy, exhibiting excellent strength and high ductility due to the formation of deformation twins at cryogenic temperatures, holds potential applications in polar districts or outer space. The investigation extends beyond the lightweight effect, examining the influence of Si addition on the microstructure and mechanical properties of CoCrNi MEA through in-situ deformation transmission electron microscopy (in-situ deformation TEM). The findings indicate that Si addition effectively reduces stacking fault energy. Deformation in CoCrNi MEA, when subjected to a single crystal under the 110 direction, primarily involves dislocation movement. In contrast, CoCrNi-Si MEA deforms through deformation twins due to its low stacking fault energy, significantly enhancing strength. The study also addresses the ongoing debate regarding the contribution of short-range order structure (SRO) to strength, finding that the formation of SRO promotes more uniform deformation. Additionally, as strain increases, the generation of deformation twins contributes substantially to strength improvement.

Keywords: AA2024 aluminum alloys; Minor Ag addition; Thermally stable  $\Omega$  phase; S phase; Warm forming; High resolution scanning transmission electron microscopy; CoCrNi medium entropy alloy; Si addition; In-situ deformation transmission electron microscope (TEM); Short-range order; Deformation twin



## First-Authored Publications Addressed in This Thesis

### Published

1. **Tai, C. L.**, Lin, Y. X., Tseng, C. Y., Chung, T. F., Yang, Y. L., Tsao, T. C., ... & Yang, J. R. (2024). Effects of different combinations of artificial ageing and warm forming on  $\Omega$  phase and S phase evolutions in an Al-5.1 Cu-1.0 Mg-0.4 Ag high strength aluminum alloy. *Materials Science and Engineering: A*, 146254.
2. **Tai, C. L.**, Chen, M. C., Chung, T. F., Yang, Y. L., Lee, S. L., Tsao, T. C., ... & Yang, J. R. (2023). The nano-structural characterization of  $\Omega$  and S phases in Al-5.1 Cu-1.0 Mg-(0.4 Ag) AA2024 aluminum alloys. *Materials Science and Engineering: A*, 145361.
3. **Tai, C. L.**, Pua, Y. M., Chung, T. F., Yang, Y. L., Chen, H. R., Chen, C. Y., ... & Yang, J. R. (2023). The effect of minor addition of Mn in AA7075 Al-Zn-Mg-Cu aluminum alloys on microstructural evolution and mechanical properties in warm forming and paint baking processes. *International Journal of Lightweight Materials and Manufacture*, 6(4), 521-533.

### In revision

1. **Tai, C. L.**, You, J. D., Chen, J. J., Liang, S. C., Chung, T. F., Yang, Y. L., II, S., Ohmura, T., Zheng, X. Y., ... & Yang, J.R. In-situ transmission electron microscopy investigation of the deformation mechanism in CoCrNi and CoCrNiSi<sub>0.3</sub> nanopillars. *Scripta Materialia*.

## Contents

口試委員審定書.....	i
誌謝.....	ii
中文摘要.....	iv
Abstract.....	vi
First-Authored Publications Addressed in This Thesis .....	viii
Contents.....	ix
List of Figures.....	xiii
Chapter 2 – General Literature Review .....	xiii
List of Tables .....	xxii
Chapter 1 – Introduction.....	1
Chapter 2 – General Literature Review .....	3
2.1 Development of Aluminum Alloys .....	3
2.1.1 Introduction.....	3
2.1.2 Effects of Minor Solute Elements Addition on Precipitate in Aluminum Alloys .....	5
2.1.3 Advanced Ageing Treatments with Different Purposes for Aluminum Alloys .....	10
2.2 Precipitates in 2xxx Al-Cu-Mg-(Ag) Aluminum Alloys .....	14
2.2.1 Introduction.....	14
2.2.2 Precipitates in AA2024 Al-Cu-Mg Aluminum Alloys.....	16
2.2.3 Precipitates in AA2040 Al-Cu-Mg-Ag Aluminum Alloys .....	22
2.3 Effects of Pre-strain on Precipitates in the 2xxx Aluminum Alloys .....	32

2.3.1 Introduction .....	32
2.3.2 Effects of Dislocation Introduction on nano-precipitates in AA2040 Aluminum Alloys .....	32
2.4 High/Medium Entropy Alloys.....	39
2.4.1 Introduction .....	39
2.4.2 Principles of High-Entropy Alloys.....	41
2.4.3 Twin .....	44
2.4.2 Effects of Solute Elements Addition in High/Medium Entropy Alloys.....	50
2.4.3 Effects of Short-Range Order Structure in High/Medium entropy Alloys.....	53
<b>Chapter 3 – General Experimental Procedures.....</b>	<b>56</b>
3.1 Materials.....	56
3.1.1 The AA2024 and AA2040 Aluminum Alloys .....	56
3.2.1 The CoCrNi-(Si) Medium Entropy Alloys.....	56
3.2 Instruments for Microstructure Analysis.....	57
3.2.1 Transmission Electron Microscope (TEM).....	57
3.2.2 Double Cs-corrected High Angle Annular Dark Field Scanning Transmission Electron Microscopy (Double Cs-corrected HAADF-STEM). .....	58
3.2.3 In-situ deformation Transmission Electron Microscope (in-situ deformation TEM) .....	58
<b>Chapter 4 – Investigations of Evolutions of <math>\Omega</math> and S phases and Mechanical Properties in low Cu/Mg weight ratio Al-Cu-Mg-(Ag) aluminum alloys.....</b>	<b>62</b>
4.1 Introduction .....	62
4.2 Experimental Procedure .....	64
4.3 Results .....	67
4.3.1 Mechanical properties .....	67

4.3.2 TEM Analysis of Alloy 0A .....	70
4.3.3 Analysis of 12 variants of S phase .....	75
4.3.4 TEM Analysis of Alloy 4A .....	78
4.3.5 TEM Analysis of S phase.....	82
4.3.6 HR-(S)TEM crystallographic Analysis .....	85
4.4 Discussion .....	89
4.4.1 Relationship between nano-precipitates and mechanical properties .....	89
4.4.2 The effect of Ag addition on the S phase .....	93
4.5 Summary .....	100

## **Chapter 5 – Effects of four different combinations of artificial ageing and warm forming on $\Omega$ phase and S phase evolutions**

### **in an Al-5.1Cu-1.0Mg-0.4Ag high strength aluminum alloy 102**

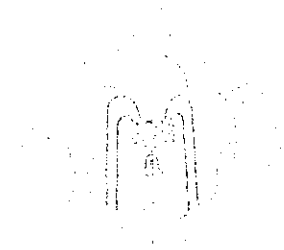
5.1 Introduction .....	102
5.2 Experimental Procedure .....	104
5.3 Results .....	107
5.3.1 Vickers hardness tests .....	107
5.3.2 TEM analyses of the $\Omega$ phase under four processes.....	109
5.3.3 TEM analyses of the S phase obtained from four different processes .....	112
5.4 Discussion .....	117
5.5 Summary .....	120

## **Chapter 6 – In-situ nano-compression testing of strengthening ability of short-range order in a CoCrNi nanopillar .....**

6.1 Introduction .....	122
6.2 Experimental Procedure .....	123
6.3 Results .....	126

6.3.1 Initial structures of CoCrNi and CoCrNiSi <sub>0.3</sub> nanopillars .....	126
6.3.2 Unaged CoCrNi nanopillar.....	128
6.3.3 Aged CoCrNi nanopillar .....	131
6.4 Discussion .....	134
6.5 Conclusions .....	138
<b>Chapter 7 – In-situ transmission electron microscopy</b>	
<b>investigation of the deformation mechanism in CoCrNi and</b>	
<b>CoCrNiSi<sub>0.3</sub> nanopillars .....</b>	<b>139</b>
7.1 Introduction .....	139
7.2 Experimental Procedure .....	140
7.3 Results and Discussion.....	141
7.3.1 Initial structures of CoCrNi and CoCrNiSi <sub>0.3</sub> nanopillars .....	141
7.3.2 In-situ compression TEM test of CoCrNi nanopillar .....	142
7.3.4 Final stage of CoCrNi and CoCrNiSi <sub>0.3</sub> nanopillars.....	148
7.4 Summary .....	151
<b>Chapter 8 General Conclusions .....</b>	<b>152</b>
<b>Chapter 9 Future Works .....</b>	<b>155</b>
<b>Reference.....</b>	<b>156</b>

## List of Figures



### Chapter 2 – General Literature Review

- Fig. 2-1. STEM images with EDS mapping of dispersoids in Alloy 7075Mn. The Mn addition facilitates the formation of dispersoids, resulting in acceleration of GPII zone and  $\eta'$  around them [18]...... 8
- Fig. 2-2. TEM images and their corresponding select area diffraction patterns of (a)  $T_1$  phase [25] and (b)  $\Omega$  phase [26]. ..... 9
- Fig. 2-3. Schematic diagrams of Retrogression and re-ageing (RRA) process. Firstly, the T6 condition is applied. Secondly, the material is placed at a higher temperature for a short period of time to re-dissolve precipitates. Despite the decrement of hardness at this stage, discontinuous precipitates at the grain boundary become prevalent, enhancing the stress corrosion resistance. Finally, re-ageing treatment, is the same as the first ageing treatment of T6 and achieves the final desired properties ..... 12
- Fig. 2-4. Schematic diagrams of warm forming and paint baking processes. In this process, warm forming combines the second step of RRA with forming process. Paint baking replaces the third step of the RRA..... 14
- Fig. 2-5. Structures and orientation relationships of precipitates in 2xxx aluminum alloys, namely  $\theta'$ , S, and  $\Omega$  phases [22, 54-58]. ..... 15

Fig. 2-6. HR-STEM images of (a)-(c) T phase and (d) S phase, which grows at the boundary of T phase [13].	18
Fig. 2-7. HAADF-STEM images of (a)-(c) different types of GPB zones and (d)-(f) their simulated structures [83].	20
Fig. 2-8. HAADF-STEM images of (a)-(d) SI and SII types S phases and (e)-(f) their simulated structures [83].	21
Fig. 2-9. The thickness of $\Omega$ phase at different ageing temperatures and holding times, from 200-300 °C and 0-1000 h, respectively [87].	23
Fig. 2-10. 3DAP element mapping of the evolution of $\Omega$ phase, revealing the gradually segregation of Ag and Mg at the boundary [91].	28
Fig. 2-11. The HR-STEM and EDS mapping images of the in-situ transformation mechanism between $\Omega'$ phase and $\Omega$ phase [94].	30
Fig. 2-12. The age-hardening curves of 0 % and 2.5 % pre-stretched samples of Al-Cu-Mg-Ag an aluminum alloy [28].	34
Fig. 2-13. APT element mapping of (a) 0 % and (b) 2.5 % pre-stretched samples and the quantification of different clusters [28].	35
Fig. 2-14. APT element mapping of (a) WQ+180 °C/10 min+1 % and (b) WQ +1 %+180 °C/10 min pre-stretched samples and the quantification of different clusters [26].	38

Fig. 2-15. The quinary high-entropy alloy FeNiCoCrMn, along with all possible quaternary and ternary medium-entropy alloys and pure element combinations, are represented with red indicating a stable FCC single-phase structure, while multiphase or other crystal structures are indicated in black. [136]..... 40

Fig. 2-16. The interactions of dislocations, electrons, phonons, and X-rays passing through a severely distorted lattice. [142] ..... 43

Fig. 2-17. Bright-field TEM image of the hierarchical annealing twin architecture in CoCrNi MEA [128]. ..... 45

Fig. 2-18. TEM images of nano-annealing twins with thicknesses less than 50 nanometers in an Fe<sub>22</sub>Co<sub>22</sub>Ni<sub>22</sub>Cr<sub>22</sub>Mn<sub>14</sub> high-entropy alloy [121]. ..... 46

Fig. 2-19. (a) TEM image of stacking fault and deformation twin forming at room temperature [128]. (b) HR-TEM image of deformation twin which formed nano-blocks under high-strain-rate deformation, leading to dynamic grain refinement [121]. ..... 48

Fig. 2-20. Tensile stress-strain curves of equiatomic (a) CoCrFeMnNi [122] and (b) CoCrNi [129] at different temperatures, range from room temperature to 77 K. .... 49

Fig. 2-21. (a) HR-TEM image of SFs, DTs and HCP structure after fracture at 77 K in a CoCrNiSi<sub>0.2</sub> MEA. (b) The enlarged image of (a). (c) The corresponding diffraction pattern [159]. ..... 52



Fig. 2-22. HR-STEM image of short-range order structure and the corresponding atomic EDS mapping for Co, Cr, and Ni [173].	53
--	----

### **Chapter 3 – General Experimental Procedures**

Fig. 3-1. Schematic diagram of twin-jet polishing instrument.	57
Fig. 3-2. (a) EBSD inverse pole figure and pole figure of 110 and 100 poles. (b) Hardness marks which located the selected grain and pole.	60
Fig. 3-3. (a) The schematic diagram of the mesh and nano-pillars. (b) The real mesh and (c) nano-pillars in SEM.	60
Fig. 3-4. The process of preparing nano-pillars from bulk material to in-situ deformation mesh by focus ion beam (FIB).	61

### **Chapter 4 – Investigations of Evolutions of $\Omega$ and S phases and Mechanical Properties in low Cu/Mg weight ratio Al-Cu-Mg-(Ag) aluminum alloys**

Fig.4-1. The illustration of the $\Omega$ phase distribution within and extending beyond the aluminum thin foil.	66
Fig.4-2. Age-hardening curves of Ag-free (Alloy 0A) and Ag-containing (Alloy 4A) samples aged at 185 °C for different holding times from 0 to 100 h.	69
Fig.4-3. TEM images of the morphologies of nano-precipitates and their diffraction patterns observed along the $[001]_{Al}$ zone axis in Alloy 0A specimens aged for (a) 5 h, (b)	

11 h (T6) and (c) 18 h (T7); STEM image observed along the  $[001]_{Al}$  zone axis for (d) 100 h. The red arrows refer to the S phase with edge-on configuration, while the green arrows, the S phase with non-edge-on configuration (denoted as S bundles). Some brighter particles in (d) due to the T phase overlapping with the S phase..... 73

Fig.4-4. (a) A HAADF-STEM image of the sample 4A-100h observed along the  $[001]_{Al}$  zone axis, (b) an enlarged image from red dotted square in (a), and the corresponding EDS mapping images of (c) Mg, (d) Cu, (e) Al and (f) Mn elements. T phase indicated by T in (f), rich in Mn..... 77

Fig.4-5. Morphologies of nano-precipitates observed along the  $[110]_{Al}$  zone axis in Alloy 4A specimens. TEM images and the corresponding diffraction patterns for Alloy 4A samples aged at 185 °C for (a) 5 h, (b) 11 h (T6), and (c) 18 h (T7). (d) STEM image of Alloy 4A specimen aged at 185 °C for 100 h. Plots (e, f) of average size and volume percent of the  $\Omega$  phase versus ageing time (5 h, 11 h, 18 h, and 100 h)..... 81

Fig.4-6. TEM images of nano-precipitate morphologies observed near the  $[001]_{Al}$  zone axis in Alloy 0A specimens: (a) 5 h, (b) T6, (c) T7, (d) 100h; and Alloy 4A specimens: (e) 5 h, (f) T6, (g) T7, and (h) 100h. The edge-on S phase (denoted as S) indicated by the red arrows, while the non-edge-on S phase (denoted as S bundles), the green arrows. .... 84

Fig.4-7. HR-TEM images of the S phase with corresponding FFT diffractograms and

simulated diffraction patterns observed along the  $[001]_{Al}$  zone axis in (a) 0A-T6 and (b) 0A-T7 specimens..... 87

Fig.4-8. The  $\Omega$  phase ageing at 185 °C for 100 h. (a) A filtered HAADF-STEM image with its (b) corresponding FFT diffractograms with the gray circle filter, (c) atomic distribution [94], and (d) simulated diffraction pattern. .... 88

Fig.4-9. High magnification TEM images of clusters observed along the  $[001]_{Al}$  zone axis in Alloy 0A specimens:(a) 5 h, (b) T6, (c) T7, and (d) 100 h ageing; and Alloy 4A specimens: (e) 5 h, (f) T6, (g) T7, and (h) 100 h ageing. .... 98

Fig.4-10. HR-TEM images with corresponding FFT diffractograms of (a) Cu-Mg clusters observed along the  $[001]_{Al}$  zone axis in a 0A-100h specimen and (b) Ag-Mg clusters observed along the  $[110]_{Al}$  zone axis in a 4A-T7 specimen. .... 99

**Chapter 5 – Effects of four different combinations of artificial ageing and warm forming on  $\Omega$  phase and S phase evolutions in an Al-5.1Cu-1.0Mg-0.4Ag high strength aluminum alloy**

Fig. 5-1. Schematic diagrams of four heat treatments. The specimens were first solid solution treated at 515 °C for 2 h, followed by natural ageing at ambient temperature for 4 days to achieve the T4 condition. Subsequently, simulated warm forming combined with artificial ageing treatment at 200 °C was carried out in the 4 combinations on the right side: (i) before artificial ageing treatment (denoted as 5%+1h), (ii) pre-aged for 20

min (denoted as 20 min+5%+40 min), (iii) pre-aged for 40 min (denoted as 40 min+5%+20 min), and (iv) after artificial ageing treatment (denoted as 1h +5%). ..... 106

Fig. 5-2. Vickers hardness (HV) values with their standard deviations for the 5 heat treatments, namely 5%+1h, 20 min+5%+40 min, 40 min+5%+20 min, 1h+5% and peak ageing (1 h) treatment. .... 108

Fig. 5-3. TEM images and their diffraction patterns observed along the  $[110]_{Al}$  zone axis for the samples: (a) 5%+1h, (b) 20 min+5%+40 min, (c) 40 min+5%+20 min and (d) 1h+5%. .... 111

Fig. 5-4. Average sizes and volume percents of the  $\Omega$  phase of the four different combinations: 5%+1h, 20 min+5%+40 min, 40 min+5%+20 min and 1h+5% treatments. .... 112

Fig. 5-5. TEM images taken near the  $[100]_{Al}$  zone axis of the morphologies of the samples: (a) 5%+1h, (b) 20 min+5%+40 min, (c) 40 min+5%+20 min and (d) 1h+5%. .... 115

Fig. 5-6. Average number densities of the rod-like S phase, lath-like S phase, and small clusters in the four different combinations: 5%+1h, 20 min+5%+40 min, 40 min+5%+20 min and 1h+5% treatments. .... 116

## **Chapter 6 – In-situ nano-compression testing of strengthening ability of short-range order in a CoCrNi nanopillar**

Fig. 6-1. (a) EBSD inverse pole figure and pole figure. (b) The thin plate on a Mo mesh.

(c) SEM image of nano-pillars. (d) TEM image of the nano-pillar before deformation. (e) Two-beam condition,  $g = [110]$ . ..... 125

Fig. 6-2. SADs observed along  $[112]$  zone axis of the (a) BF-TEM images of the unaged CoCrNi and (b) DF-TEM images of the aged CoCrNi nanopillars prior to deformation. .... 127

Fig. 6-3. Unaged CoCrNi nanopillar's (a) Stress–strain curve. The corresponding TEM images of points (b)-(f) in the stress-strain curve, presenting the evolution of the deformation behavior through slip bands. .... 130

Fig. 6-4. Aged CoCrNi nanopillar's TEM images of points (a)-(f) in the stress-strain curve, illustrating the microstructural evolution of slip bands in the nanopillar. .... 133

Fig. 6-5. (a) The final stage TEM image of the unaged CoCrNi nanopillar. (b) The enlarged image from (a). (c) The final stage TEM image of the aged CoCrNi nanopillar. (d) The enlarged image from (c). .... 137

**Chapter 7 – In-situ transmission electron microscopy investigation of the deformation mechanism in CoCrNi and CoCrNiSi<sub>0.3</sub> nanopillars**

Fig. 7-1. TEM images of the (a) CoCrNi and (b) CoCrNiSi<sub>0.3</sub> nanopillars prior to deformation. ....141

Fig. 7-2. CoCrNi nanopillar's (a) Stress–strain curve. TEM images of (b)-(f) strain burst

with escape of dislocations and formation of slip bands in the nanopillar. ....144

Fig. 7-3. CoCrNiSi<sub>0.3</sub> nanopillar's (a) Stress–strain curve. TEM images of (b)-(d) deformation twins impeding dislocations, and (e) and (f) strain bursts with escape of deformation twins and dislocations in the nanopillar. ....147

Fig. 7-4. (a) The final stage TEM image of the CoCrNi nanopillar. (b) The enlarged image from (a). (c) The final stage TEM image of the CoCrNiSi<sub>0.3</sub> nanopillar. (d) The enlarged image from (c). ....150

## List of Tables

Table 1. The characteristics of aluminum alloys belonging to different series [1-3].	4
Table 2. Designations of heat treatment in aluminum alloys [4].	5
Table 3 Orientation relationships between S and T phases.	18
Table 4. Orientation relationships between $\Omega$ phase and aluminum matrix.	26
Table 5. The thermodynamic model of stacking fault energy of different Si contents in CoCrNi MEA [150].	52
Table 6. Chemical compositions (in wt. %) of Al-Cu-Mg-(Ag) alloys studied.	56
Table 7. Chemical compositions (in at. %) of CoCrNi-(Si) alloys studied.	56
Table 8. YSs, UTSs, Els, and comparison of UTSs (based on T6 condition) of Alloys 0A and 4A aged at 185 °C for 5, 11 (T6), 18 (T7), and 100 h.	70
Table 9. Orientation relationships between S phase variants and aluminum matrix.	74
Table 10. The intersection directions between 12 variants of S phase and the observation plane $(001)_{Al}$ .	74